Journal of Alzheimer's Disease 85 (2022) 1233–1250
DOI 10.3233/JAD-215149
IOS Press

Studying *APOE* ε4 Allele Dose Effects with a Univariate Morphometry Biomarker

Gang Wang[a,*], Wenju Zhou[b], Deping Kong[c], Zongshuai Qu[c], Maowen Ba[d], Jinguang Hao[c], Tao Yao[c], Qunxi Dong[e,f], Yi Su[g], Eric M. Reiman[g], Richard J. Caselli[h], Kewei Chen[g] and Yalin Wang[f,*] for the Alzheimer's Disease Neuroimaging Initiative[1]
[a]*School of Ulsan Ship and Ocean College, Ludong University, Yantai, China*
[b]*School of Mechatronic Engineering and Automation, Shanghai University, Shanghai, China*
[c]*School of Information and Electrical Engineering, Ludong University, Yantai, China*
[d]*Department of Neurology, The Affiliated Yantai Yuhuangding Hospital of Qingdao University, Yantai, China*
[e]*Institute of Engineering Medicine, Beijing Institute of Technology, Beijing, China*
[f]*School of Computing and Augmented Intelligence, Arizona State University, Tempe, AZ, USA*
[g]*Banner Alzheimer's Institute, Phoenix, AZ, USA*
[h]*Department of Neurology, Mayo Clinic Arizona, Scottsdale, AZ, USA*

Accepted 4 November 2021
Pre-press 16 December 2021

Abstract.
Background: A univariate neurodegeneration biomarker (UNB) based on MRI with strong statistical discrimination power would be highly desirable for studying hippocampal surface morphological changes associated with *APOE* ε4 genetic risk for AD in the cognitively unimpaired (CU) population. However, existing UNB work either fails to model large group variances or does not capture AD induced changes.
Objective: We proposed a subspace decomposition method capable of exploiting a UNB to represent the hippocampal morphological changes related to the *APOE* ε4 dose effects among the longitudinal *APOE* ε4 homozygotes (HM, $N = 30$), heterozygotes (HT, $N = 49$) and non-carriers (NC, $N = 61$).
Methods: Rank minimization mechanism combined with sparse constraint considering the local continuity of the hippocampal atrophy regions is used to extract group common structures. Based on the group common structures of amyloid-β (Aβ) positive AD patients and Aβ negative CU subjects, we identified the regions-of-interest (ROI), which reflect significant morphometry changes caused by the AD development. Then univariate morphometry index (UMI) is constructed from these ROIs.
Results: The proposed UMI demonstrates a more substantial statistical discrimination power to distinguish the longitudinal groups with different *APOE* ε4 genotypes than the hippocampal volume measurements. And different *APOE* ε4 allele load affects the shrinkage rate of the hippocampus, i.e., HM genotype will cause the largest atrophy rate, followed by HT, and the smallest is NC.
Conclusion: The UMIs may capture the *APOE* ε4 risk allele-induced brain morphometry abnormalities and reveal the dose effects of *APOE* ε4 on the hippocampal morphology in cognitively normal individuals.

Keywords: Effect size, magnetic resonance imaging, permutation *t*-test, radial distance, regions-of-interest, subspace decomposition

[1]Data used in preparation of this article were obtained from the Alzheimer's Disease Neuroimaging Initiative (ADNI) database (http://adni.loni.usc.edu). As such, the investigators within the ADNI contributed to the design and implementation of ADNI and/or provided data but did not participate in analysis or writing of this report. A complete listing of ADNI investigators can be found at: http://adni.loni.usc.edu/wp-content/uploads/how_to_apply/ADNI_Acknowledgement_List.pdf

*Correspondence to: Dr. Gang Wang, School of Ulsan Ship and Ocean College, Ludong University, Yantai, China. Tel.: +86 535 6653786; E-mail: gangwang1970@ldu.edu.cn and Dr. Yalin Wang, School of Computing and Augmented Intelligence, Arizona State University, P.O. Box 878809, Tempe, AZ 85287, USA. Tel.: +1 480 965 6871; Fax: +1 480 965 2751; E-mail: ylwang@asu.edu.

INTRODUCTION

Alzheimer's disease (AD) is an irreversible neurodegenerative disorder characterized by progressive cognitive impairment that interferes with memory, thinking, and behavior. For AD prevention therapies to have a maximal effect, they might need to be initiated before measurable impairments in cognition, at which time extensive pathology likely already exists [1, 2]. Therefore, there is a need to study biomarkers closely related to AD progression in its earliest non-symptomatic and symptomatic stages to observe AD development and evaluate the effectiveness of early interventions. It is well known that the apolipoprotein E (*APOE*) ε4 allele is a major genetic risk factor for late-onset AD [3, 4]. Its discovery has made it possible to study large numbers of genetically at-risk individuals before the onset of symptomatic memory impairment, and has led to the concept of the preclinical stage of AD [5]. Therefore, studying the association between *APOE* genotype with neurodegenerative pathology in healthy adults may benefit the development of preclinical AD biomarkers.

Numerous studies have revealed the pathological correlations between probable AD and the *APOE* ε4 allele by using a variety of biomarkers, including magnetic resonance imaging (MRI) studies of whole brain atrophy rates of *APOE* ε4 carriers [6], fluorodeoxyglucose positron emission tomography (FDG-PET) studies of *APOE* ε4 carriers that have revealed AD-like patterns of reduced cerebral metabolic rate glucose [7, 8], measures of increased amyloid plaque burden determined from increases in the standard uptake value ratio of florbetapir PET [9], and distinct default mode network alterations observed in the resting-state functional MRI analysis [10], etc. Among them, structural MRI (sMRI) has been widely used to identify brain structure changes, including cortical atrophy [11, 12], hippocampal atrophy [13–15], or ventricular enlargement [14, 16], which can serve as the indicative diagnostic biomarkers of early AD, owing to their close relationship between neurodegeneration and cognition. Hippocampal atrophy measures from structural MRI are widely used for investigating the genetic influence of *APOE* ε4 on hippocampal morphology because the changes in hippocampal morphometry become apparent in the early stages of memory decline [13, 17–20]. However, the genetic influence of *APOE* ε4 on hippocampal morphometry research has reported mixed results. Some studies have elucidated a dose-dependent disease vulnerability on the hippocampal structure level [21–26], including our own work [27], e.g., significantly reduced hippocampal volume or accelerated longitudinal hippocampal atrophy has been found in healthy *APOE* ε4 homozygotes (HM), as compared to heterozygotes (HT) and non-carriers (NC). Some other studies [28–33] did not find significant group differences between HM, HT, and NC. Therefore, developing sensitive and reliable brain imaging biomarkers to validate the dose-dependent impact of the *APOE* ε4 allele on hippocampus among cognitively unimpaired individuals would be highly advantageous to preclinical AD diagnosis and prognosis.

While much *APOE* genetic influence on hippocampal morphometry research adopted multivariable imaging biomarkers (e.g., [26, 27]), a univariate neurodegeneration biomarker based on an individual patient's brain scans with high diagnostic accuracy would be highly desirable for clinical use [34] and patient screening in clinical trials [2]. Such a personalized measure may overcome inflated Type I error due to multiple comparisons [30, 31]. For example, for randomized clinical trials, regulatory agencies, including the Food and Drug Administration, requires conventional univariate hypothesis testing and its associated statistical power analysis [2]. Meanwhile, a single MRI-based measure of cerebral atrophy was used as a neurodegeneration biomarker in the recently proposed AD amyloid/tau/neurodegeneration framework [35]. In our recent work [36], we proposed a subspace decomposition framework to generate a univariate morphometry index to quantify the hippocampal morphological changes induced by AD based on the reliable and informative region-of-interest (ROI), which takes into account the intense image noise and the significant within-group variance on the obtained structural MR images. However, our previous algorithm for solving stable principal component pursuit (SPCP) has few limitations. First, our previous work's low-rank subspace decomposition algorithm is the alternating splitting augmented Lagrangian method (ASALM). The disadvantage of ASALM is that its convergence is slow for real-time application [37]. Second, the singular value decomposition (SVD) in our previous algorithm used a low-rank matrix factorization mechanism to factorize a large-sized matrix into two small-sized matrices generated by implementing matrix column orthogonal strategy and low-rank constraint. Although this mechanism can effectively reduce the SVD computation cost for a large-scale matrix, the excessive

intermediate processing steps require further optimization.

In this work, we propose an improved subspace decomposition framework to establish univariate and personalized neurodegeneration MRI biomarkers with strong statistical discrimination power [34]. We hypothesize that the proposed univariate morphometry biomarker may distinguish hippocampal surface morphological changes related to the *APOE* ε4 dose effects in the cognitively unimpaired population. In our experiments, we first used sMRI images of 120 Aβ positive AD patients and 257 Aβ negative CU subjects from the Alzheimer's Disease Neuroimaging Initiative (ADNI) cohort [38] to establish the AD-specific abnormality patterns over the hippocampal surface. We then compute a univariate similarity index to examine the degree of similarity to this AD-specific surface pattern for a given individual subject from an independent Arizona *APOE* cohort [39], including 140 cognitively unimpaired individuals (30 HMs, 49 HTs, and 61 NCs). We aim to test whether the proposed univariate morphometry biomarker gains improved computational efficiency and whether it has the superiority to the raw surface and volume measurements in reflecting the morphological atrophy rates caused by different *APOE* ε4 allele loads in the CU individuals.

MATERIALS AND METHODS

Subjects

Data used in the preparation of this article were partially obtained from the Alzheimer's Disease Neuroimaging Initiative (ADNI) database (http://adni.loni.usc.edu). The ADNI was launched in 2003 as a public-private partnership, led by Principal Investigator Michael W. Weiner, MD. The primary goal of ADNI has been to test whether serial MRI, PET, other biological markers, and clinical and neuropsychological assessment can be combined to measure the progression of mild cognitive impairment and early AD. For up-to-date information, see http://www.adni-info.org.

Specifically, the sMRI data used to generate AD-specific abnormality patterns, including 120 amyloid-β (Aβ) positive AD patients and 257 Aβ negative CU subjects, were downloaded from the ADNI database [38]. The reason for choosing Aβ positive subjects is that the accumulation of Aβ is one of the hallmarks of AD in human brains and a positive Aβ reading is now accepted as 'dementia due to AD' together with the presence of clinical symptoms [40].

To validate the effects of *APOE* ε4 allele load on hippocampal morphology, we used 140 cognitively unimpaired individuals from the Arizona *APOE* cohort [39] and studied longitudinal brain imaging changes via statistical group difference analysis. The Arizona *APOE* cohort was established since January 1, 1994, which contains cognitively normal residents of Maricopa County aged 21 years and older. Demographic, family, and medical history data were obtained on each individual undergoing *APOE* genotyping, and their identity was coded by a study assistant. All individuals gave their written, informed consent-approved by the Institutional Review Boards of all participating institutions-and agree to have the results of the *APOE* test withheld from them as a precondition to their participation in this study. Genetic determination of *APOE* allelic status was performed using a polymerase chain reaction-based assay [41]. All subjects were genotyped and classified as *APOE* ε4 carriers ($N_{HM} = 30$, $N_{HT} = 49$) or non-carriers ($N_{NC} = 61$). The study excludes subjects with potentially confounding medical, neurological, or psychiatric problems (such as prior stroke, traumatic brain injury, memory, or other cognitive impairment, parkinsonism, major depression, or substance abuse). No subject included in the study met the published criteria for mild cognitive impairment, AD, any other form of dementia [42].

Algorithm pipeline

We briefly summarize our overall sequence of steps used to compute the univariate morphometry biomarker. The following sections are detailed explanations of each step. Figure 1 shows the processing procedures in our system. First, we segment hippocampi from T1-weighted MR images and reconstruct hippocampal surfaces. We register hippocampal surfaces across subjects and compute surface morphometry features, radial distance (RD) [43, 44]. Second, we construct two group observation matrices (i.e., Aβ positive AD observation matrix and Aβ negative CU observation matrix) where all RD features of each registered subject are stacked as a column vector. To effectively extract the robust group common morphological structure contained in all individual RD features, we further decompose each group observation matrix into low-rank component, sparse component and noise using a subspace decomposition algorithm. The low-rank component

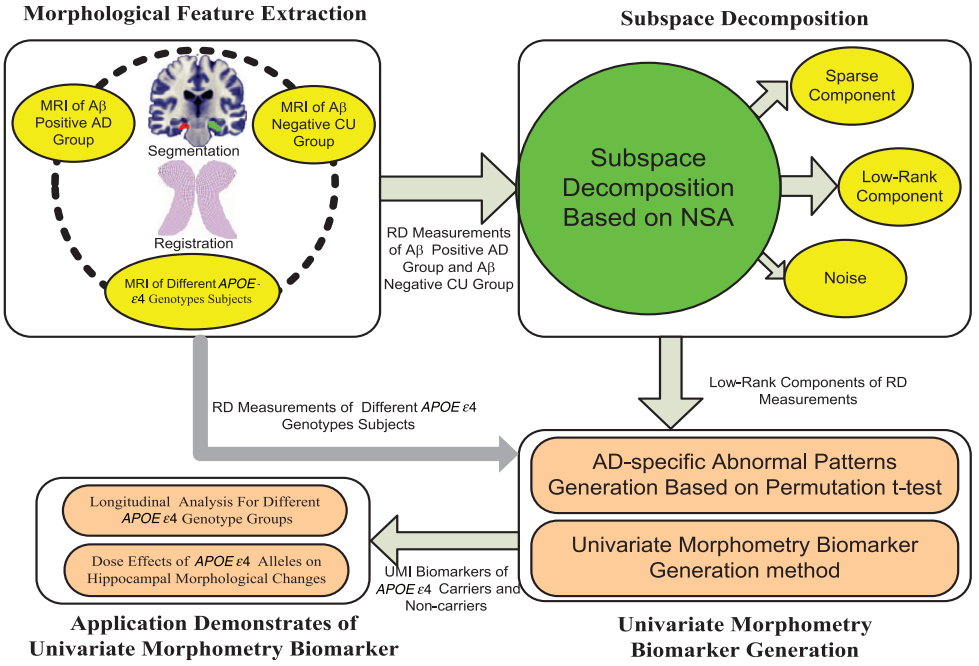

Fig. 1. Processing procedures in our univariate morphometry biomarker system.

is the group common structure contributed by all the subjects in the same group, the sparse component is the sparse diversities which belong to specific individual subjects. With the subspace decomposition framework, we may obtain the two intrinsic group common morphological structures of Aβ positive AD group and Aβ negative CU group, which takes into account the intense imaging noise and the significant within-group variance on the obtained structure MR images. Third, we compute AD-specific abnormal surface patterns on the ROIs which are identified as significantly different areas induced by AD between the low-rank components of two groups, Aβ positive AD group and Aβ negative CU group. We further use the labeled ROIs and the registration result of an individual hippocampal surface to compute the univariate morphometry index (UMI). Finally, as application demonstrations of the computed UMIs, we apply them to study the longitudinal brain imaging changes of the three *APOE* ε4 genotype groups and dose effects of *APOE* ε4 alleles on the hippocampal morphology.

Image acquisition and morphometry feature extraction

High-resolution brain structural MRI scans were acquired using 3 Tesla MRI scanners manufactured by General Electric Healthcare, Siemens Medical Solutions, and Philips Medical Systems. For each subject, a high-resolution T1 magnetization-prepared spoiled gradient (SPGR) scan was obtained in the sagittal plane. A T1-weighted pulse sequence (radiofrequency-SPGR recall acquisition in the steady state, repetition time = 33 ms, echo time = 5 ms, alpha = 30°, number of excitations = 1, field-of-view = 24 cm, imaging matrix = 256 × 93, slice thickness = 1.5 mm, scan time = 13:36 min) was used to acquire 124 contiguous horizontal MRI slices with in-plane voxel dimensions of 0.94 × 1.25 mm.

Based on the T1-weighted MRI scans, hippocampal substructures were segmented by using FIRST in the FMRIB Software Library [45] and 3D triangular hippocampal surface was reconstructed based on marching cubes algorithm [46]. With the generated conformal grid for each surface [47], we computed the hippocampal surface's conformal representation, which represents the intrinsic and extrinsic features of the surface, respectively. In addition, we carried out a surface fluid registration algorithm [48] and an inverse-consistent surface registration framework to increase robustness [47]. Then all the surfaces have a common reference frame and RD statistical morphological measurements were computed directly on these registered surfaces. RD is the distance from each surface point to its medial core

(analogous to the centerline in a tube), representing hippocampal atrophy or enlargement. The entire hippocampal surface morphometry pipeline is described in our prior work [47] and is publicly available at https://www.nitrc.org/projects/mtsms_2020.

Subspace decomposition algorithm

When all individual RD features of the same group are stacked into column vectors to form an observation matrix $A = (a_1, \ldots, a_n) \in \Re^{m\times n}$ (a_i denotes the column vector which represent RD features of i-th subject, m is the dimension of each subject RD features and n is the number of the subjects within the same group), the SPCP algorithm enables us to decompose A into low-rank component $L \in \Re^{m\times n}$, sparse component $S \in \Re^{m\times n}$, and noise $N \in \Re^{m\times n}$. In order to improve the computation efficiency, we apply Non-Smooth Augmented Lagrangian Algorithm (NSA) [49] based on partial variable splitting to solve this non-smooth convex optimization problem. It is known that the recovery is possible even when the data matrix, A, is corrupted with a dense error matrix, $\|N\|_F \le \delta$, by solving the SPCP problem [50].

$$\min_{LS\in R^{m\times n}} \{\|L\|_* + \gamma \|S\|_1,\ s.t. : \|L + S - A\|_F \le \delta\} \quad (1)$$

where $\|\cdot\|_*$ is the nuclear norm and $\|\cdot\|_1$ is the l_1 norm, which are given by $\|L\|_* = \sum_i \sigma_i(L)$ and $\|S\|_1 = \sum_{i,j} |S_{i,j}|$, respectively. And γ controls the relative importance of the low-rank term L versus the sparse term S. $\sigma_i(L)$ is the ith largest singular value of L.

Based on NSA, the subproblems for solving low-rank component L and sparse component S of Equation (1) via the following iteration procedure:

$$\begin{cases} L_{k+1} \leftarrow \arg\min_L \{\|L\|_* + \langle Y_k, L - Z_k\rangle + \dfrac{\rho k}{2} \|L - Z_l\|_F^2\} \\ (Z_{k+1}, S_{k+1}) \leftarrow \arg\min_{(Z,S)} \\ \quad \left\{\gamma \|S\|_1 + \langle -Y_k, Z - L_{k+1}\rangle + \dfrac{\rho k}{2} \|Z - L_{k+1}\|_F^2\right\} \\ Y_{k+1} \leftarrow Y_k + \rho_k(L_{k+1} - Z_{k+1}) \\ \rho_{k+1} = \alpha\rho_k,\ \alpha \ge 1 \end{cases} \quad (2)$$

Let $Y_k \in R^{m\times n}$ and θ_k be optimal Lagrangian dual variables for $Z_k = L_k$ and $\frac{1}{2}\|Z + S - A\|_F^2 \le \frac{\delta^2}{2}$ constraints, $\rho_k > 0$ is the penalty parameter for the violation of the linear constraint and $\langle . \rangle$ denotes the standard trace inner product. In procedure (2), the subproblem for computing L_{k+1} is a matrix shrinkage problem which can be solved via thresholding the singular values of the matrix $(Z_k - Y_k/\rho_k)$ [51]. And the subproblem for computing S_{k+1} is an element shrinkage problem which can be solved via l_1 norm:

$$S_{k+1} = sign\,(A - (L_{k+1} + Y_k/\rho_k)) \odot \max\left\{\left|A - \left(L_{k+1} + \frac{\gamma_k}{\rho k}\right)\right| - T_{th}, 0\right\} \quad (3)$$

where T_{th} is the threshold which is defined as $T_{th} = (\rho_k + \theta_k)/(\sqrt{\max(m,n)} \cdot \rho_k \cdot \theta_k)$, $\{\theta_k\}_{k\in z^+}$ is a bounded sequence, and θ_k satisfies the following expression $\delta = \left\|\min\left\{\frac{\gamma}{\theta k}E,\ \frac{\rho k}{\rho k + \theta k}\left|A - (L_{k+1} + \frac{1}{\rho k}Y_k)\right|\right\}\right\|_F$, $\odot$ denotes the componentwise multiplication operator. The details about computing L_{k+1} based on improved partial SVD and computing S_{k+1} by considering the local continuity of the hippocampal atrophy regions can be found in the Supplementary Material. Based on the description above, we can use the proposed method to recover the low-rank component and the sparse component with the local continuous constraint from the large-scale data matrix under the complicated environment. In particular, we can use the low-rank component L, i.e., the essential group common structure, to detect the group differences without the influence of the individual's specific diversities S and noise.

Univariate morphometry index for AD-specific abnormal surface pattern similarity measure

A UMI reflecting individual AD-specific abnormal surface pattern similarity is generated by summarizing information in ROIs. Our UMI generation procedure is similar to our prior work [36]. First, for each registered vertex on the hippocampal surface, we used permutation t-test [52] to analyze the group difference for the low-rank components of the RD features between Aβ positive AD group and Aβ negative CU group. Given the level of significance α, the accepted vertices to form the ROIs can be obtained for their permutation p-maps with the probabilities $< \alpha$. Since the extracted low-rank components represent the common morphological structure of the group, the extracted ROIs based on low-rank components obtained by subspace decomposition algorithm can accurately reflect the hippocampal morphological structure changes from CU to AD.

Secondly, we use a vertex-wise two-sample independent *t*-test for the mean differences between the low-rank components of the Aβ negative CU and the Aβ positive AD groups on the predefined ROIs. The obtained *t*-map is then transformed into a *z*-score map which is called as AD-specific abnormal surface pattern. And a vertex-wise two-sample independent *t*-test is applied for the differences between raw RD measures of individual subject and the mean low-rank components of the Aβ negative CU group on the predefined ROIs. The obtained *t*-map is then transformed into a *z*-score map which is called as individual atrophy degree. At last, the UMIs can be computed through the vertex-wise summation across all the vertices on the predefined ROIs with the production of AD-specific abnormal surface patterns and the atrophy degrees of the individual subject. Thus,

$$UMI = \frac{\sum_{i=1}^{m}(D_{Ti} \cdot D_{Wi})}{100} \quad (4)$$

Here D_{Ti} denotes the atrophy degree at vertex i of the individual subject, D_{Wi} is the AD-specific abnormal surface pattern at vertex i between the AD group and the CU group. From the Eq. (4), we can see that the UMI measures the degree of similarity to this AD-specific abnormal surface pattern for a given individual subject on the selected ROIs. In other words, the greater the UMI, the closer the atrophy degree of the individual subject is from AD morphological characteristics.

Evaluation of the univariate biomarkers

For longitudinal cognitively unimpaired *APOE* ε4 carriers (HM and HT) and non-carriers (NC) groups, we analyze the longitudinal group changes of the univariate biomarkers, including the UMIs, Mini-Mental State Examination (MMSE) [53] scores, Auditory Verbal Learning Test Long-Term Memory (AVLT-LTM) [54] scores and hippocampal volume measures, to compare the statistical discrimination abilities of different univariate biomarkers based on analysis of variance (ANOVA) method. All subjects of each longitudinal group underwent two tests, including the baseline test and a 24-month test. Meanwhile, Cohen's d test is applied to evaluate the effect size of the univariate biomarkers above. Cohen's d test takes the difference in means between two groups and is divided by the pooled standard deviation of the groups.

To further assess the statistical powers of the univariate biomarkers, we calculate the required minimum sample sizes (MSS) by comparing the univariate biomarker means of each longitudinal *APOE* ε4 genotype groups at two test time points (baseline test and 24-month test). Suppose the means and standard deviations of the specific univariate biomarker of each longitudinal group at two test time points are (μ_1, σ_1) and (μ_2, σ_2). To conduct a two-sided test with significance level α and power of 1-β, the appropriate sample-size for the specific univariate biomarker is as follows [55]:

$$MSS = \frac{\left(\sigma_1^2 + \sigma_2^2\right)\left(z_{1-\alpha/2} + z_{1-\beta}\right)^2}{\Delta^2} \quad (5)$$

where $\Delta = |\mu_2 - \mu_1|$. The significance level α is set as 0.05 and the power 1-β is set as 0.8. For each longitudinal group, if the MSS derived from A biomarker is smaller than B biomarker, we can conclude that A biomarker is more differentiated than B biomarker. This indicates that MSS is an indicator for characterizing the statistical identification ability of the biomarkers.

Table 1
Demographic information of Aβ positive AD and Aβ negative CU groups, from the ADNI cohort

	AD	CU	Inferential Statistics
Sample Size	120	257	
Gender (M/F)	64/56	125/132	$\chi^2 = 0.7214$; $p = 0.40$
Age	74.15 ± 7.47	75.24 ± 6.45	$F = 2.13$; $p = 0.15$
Education	15.61 ± 2.69	16.10 ± 2.50	$F = 2.94$; $p = 0.09$
MMSE	22.53 ± 3.25	28.93 ± 2.20	$F = 503.67$; $p < 0.0001$

RESULTS

ROIs extraction

In order to extract the significant morphological group differences induced by AD, we apply the subspace decomposition to a cohort consisting of 120 Aβ positive AD patients and 257 Aβ negative CU subjects from the ADNI database. Demographic and clinical data of this cohort is compared using a one-way analysis of variance, and the gender data was analyzed by a chi-square test. Table 1 indicates that the factors of age, gender, and education of these two groups are matched, while the MMSE is significantly different between these two groups.

Table 2
The performance indicators for the left and right hippocampus based on subspace decomposition algorithm (with data from the ADNI cohort)

		ρ_0	rank(L)	$\|S\|_{\Omega,1}$	$\|L+S-A\|/\|A\|$
Left Hippocampus	CU	0.09	11∼12	142∼150	0.056
	AD	0.13	9∼11	209∼225	0.057
Right Hippocampus	CU	0.08	11∼12	146∼153	0.057
	AD	0.12	9∼11	218∼226	0.058

Because low-rank components correspond to group common morphological structures, we apply subspace decomposition algorithm to extract the low-rank component of Aβ positive AD and Aβ negative CU observation matrices, respectively. Each observation matrix is formed by stacking individuals of each group. Considering the bias and variance of the ROI generation model, we randomly divide the subjects of each group into 10 folds and choose 9 folds from each group as the training sets respectively. This process is repeated 10 times. The purpose of this process is to validate if the generated ROIs each time is consistent. The total performance indicators for the left and the right hippocampus based on our algorithm are shown in Table 2. Here we set the parameter γ as 0.0082. From the performance indicators in Table 2, the parameters setting ρ_0, rank(L) and $\|L+S-A\|/\|A\|$ of each group (Aβ positive AD group or Aβ negative CU group) is similar whether it is on the left or the right hippocampus. Here the rank of L is obtained by counting the number of the eigenvalues of L whose values are greater than three times the δ. Here $\delta = 0.15$.

After extracting the L and S from the observation matrix A, we can define the ROIs by using permutation t-test between the L of Aβ positive AD group and the L of Aβ negative CU group. As the training samples are taken randomly each time (the changing rate is about 10%), each ROI obtained will be inconsistent if the extracted L components are not robust.

In order to verify whether the ROIs generated by the L components are robust, we imitated the process of generating the ROIs based on the L components, and formed the ROIs based on the raw RD features of Aβ positive AD group and Aβ negative CU group, then verify whether the ROIs generated by each type of data (L components or raw RDs) are consistent when the training data is different at each time.

In addition, to improve the computational efficiency, we run Monte Carlo to generate two random groups for each registered sample point on the surface, which takes relatively small random permutation processes of the possible replicates. Here the number of random permutation processes is set as 5,000. Moreover, the generated ROIs are the vertices whose permutation t-test p-values (uncorrected for multiple comparisons) representing the group differences are smaller than 0.00001. The generated ROIs of the left hippocampus (LH) and right hippocampus (RH) based on the low-rank components and the RD data are shown in Fig. 2. Figure 2a and 2b are the statistical ROI results for LH. Figure 2c and 2d are the statistical ROI results for RH. Furthermore, Fig. 2a and 2c are the statistical ROI results based on the low-rank components. Figure 2b and 2d are the statistical ROI results based on the raw RD data. Non-blue colors show the number of times a vertex is selected. The red color denotes that the vertex is selected 10 times after 10 ROI generation processes. For LH, the total number of ROI vertices based on the low-rank components is 2,162, and the vertices having been selected 10 times account for 75.28% of the total number of ROI vertices, while they are 2,542 and 52.41% based on the raw RD data. For the right hippocampus, they are 2,249 and 74.23% based on the low-rank component, 2,518 and 54.23% based on raw RD data. From the results, we can see that the selected ROIs based on the low-rank component are more robust than the ROIs based on the raw RD data. It suggests that the low-rank component can represent the essential common structure from the subjects without the interference of the unique individual structure and the noise.

In our previous work [36], we used the subspace decomposition algorithm (ASALM) to extract low-rank components and sparse components based on stable principal component pursuit which are combined with a low-rank matrix factorization mechanism [56]. This paper used the subspace decomposition algorithm (NSA) to extract low-rank components and sparse components based on a stable principal component pursuit combined with a partial SVD mechanism. Both mechanisms are to speed up the SPCP optimization for large-scale matrices by avoiding the full SVD computation. Moreover, the low-rank components extracted by the two methods have the same rank and high similarity. However, the NSA algorithm has a faster convergence rate, i.e., fewer iteration steps, than the ASALM algorithm. A brief convergence speed comparison of the two algorithms is presented in Fig. 3. All the experiments are performed with an Intel Core i7 personal computer,

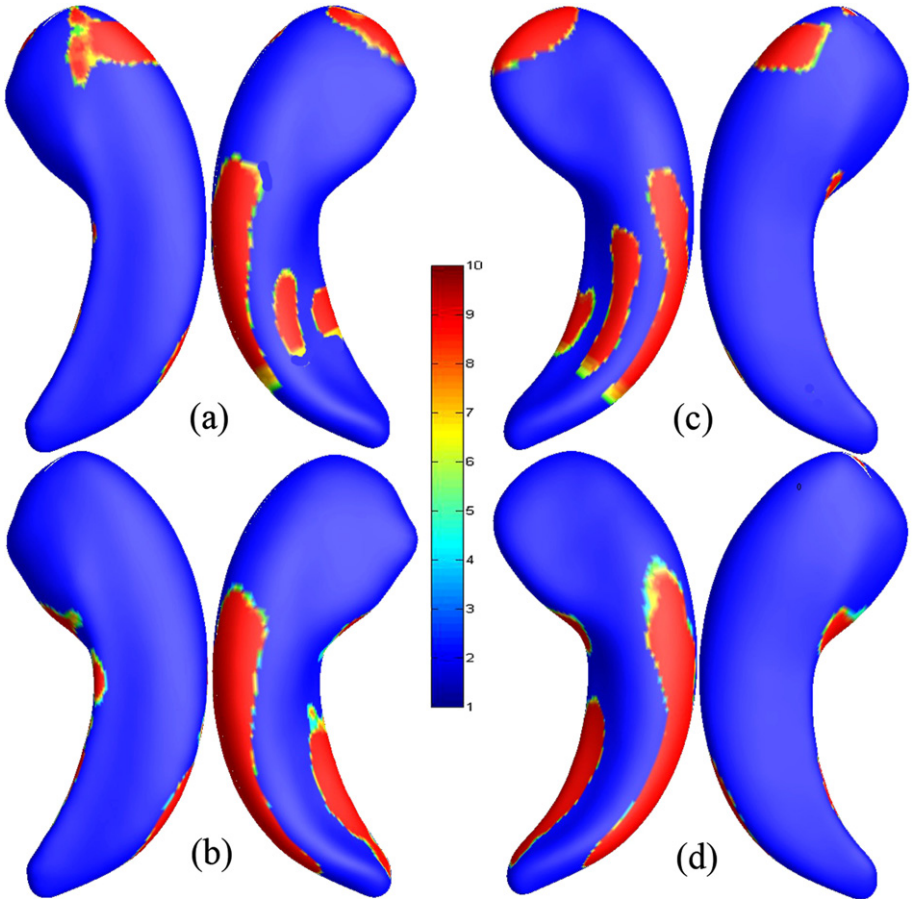

Fig. 2. The extracted ROIs for the group differences between Aβ positive AD group and Aβ negative CU group based on the low-rank data and the RD data. (a) and (b) are the statistical ROI results for LH. (c) and (d) are the statistical ROI results for RH. And (a) and (c) are the statistical ROIs based on the low-rank components. (b) and (d) are the statistical ROIs based on the RD data. All the statistic ROI results are obtained by the permutation *t*-test ($p < 0.00001$, uncorrected for multiple comparisons). Non-blue colors show the number of times a vertex is selected.

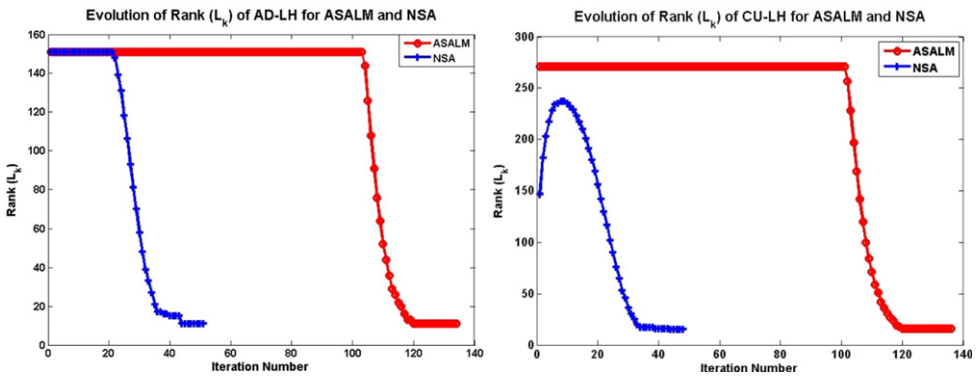

Fig. 3. Evolution of rank(L_k) for ASALM and NSA algorithms.

with 3.40 GHz CPU, 16 GB RAM and MATLAB 2016 installed in the Win 7 operating system. With the same termination condition, the evolution of rank (L_k) for extracting low-rank components of left hippocampus of AD group shows that the results showed that the extracted low-rank components of AD-LH

Table 3
Demographic information of the different longitudinal genotype groups, from the AZ *APOE* cohort. Means are followed by standard deviations for education, age, and MMSE measurements

		Gender (M/F)	Education	Age	MMSE
HM baseline		8/22	16.21 ± 2.18	65.01 ± 5.38	29.75 ± 0.58
HM m24				67.37 ± 5.43	29.54 ± 0.81
HT baseline		16/33	15.72 ± 2.41	68.01 ± 6.69	29.58 ± 0.79
HT m24				70.24 ± 6.64	29.58 ± 1.03
NC baseline		18/43	15.92 ± 2.24	66.64 ± 7.01	29.71 ± 0.59
NC m24				68.85 ± 6.94	29.68 ± 0.66
Inferential Statistics	baseline	$\chi^2 = 0.33$; $p = 0.85$	$F = 0.38$; $p = 0.68$	$F = 1.21$; $p = 0.30$	$F = 0.59$; $p = 0.56$
	m24			$F = 1.14$; $p = 0.32$	$F = 1.28$; $p = 0.28$

and CU-LH groups based on the two methods have the same ranks, that is, the rank equals to 10 for AD-LH and 13 for CU-LH. Using Corr2 in Matlab, we obtained that the correlation between the two low-rank components based on the two methods is 0.992 for AD-LH, and 0.994 for CU-LH. To extract the final low-rank components, the iteration number of the NSA method accounts for about 38% of the ASALM method. The NSA with a partial SVD mechanism is more efficient than the ASALM with a low-rank matrix factorization mechanism.

Longitudinal study for different APOE ε4 genotype groups

There are 140 cognitively unimpaired individuals with 61 NCs, 49 HTs, and 30 HMs from the Arizona *APOE* cohort. All subjects underwent two tests, including the baseline test and a 24-month test. Through the comparisons between the demographic and clinical data of the different groups at these two test time points, the statistical results in Table 3 indicate that there are no significant group differences in the factors of gender, education degree, age, and MMSE between the three groups.

Based on the predefined ROIs from the low-rank components of Aβ positive AD group and Aβ negative CU group determined above, we generated the UMIs of the cognitively unimpaired individuals with different *APOE* ε4 genotypes (HM, HT, and NC) at two test points (baseline test and 24-month test) and studied the statistical differentiation ability of the UMIs for the different longitudinal groups. Specifically, since the predefined ROIs represent the significant group difference areas induced by AD, the generated UMIs indicate the degree of similarity to the AD-specific abnormal surface pattern for a given individual subject with different *APOE* ε4 genotypes before the onset stage of AD. Combined the AD-specific abnormal surface patterns and the individual atrophy degrees on the selected ROIs, the UMIs of the cognitively unimpaired individuals with different *APOE* ε4 genotypes can be computed through Equation (4). In order to verify whether the generated UMIs have strong statistical power for distinguishing these three longitudinal groups, we introduce the UMIs based on raw RD measures (UMI-RD) and the volume data to compare the discrimination power with the UMIs based on the subspace decomposition. The UMI-RDs of the different *APOE* ε4 subjects are computed according to Equation (4) based on the obtained ROIs shown in Fig. 2b and 2d. The volumetric MRI measurements of the hippocampus are generally accepted as the best-established biomarkers of clinical AD progression [57]. Moreover, the hippocampal volume is computed on our smoothed surfaces after linearly registered to the MNI imaging space [58].

Table 4
The longitudinal study from baseline to 24-month follow-up for different *APOE* ε4 genotype groups (from the AZ *APOE* cohort) based on different univariate biomarkers

Biomarker	genotype	MSS	Effect Size
UMI	NC	533	0.48
	HT	393	0.53
	HM	296	0.61
UMI-RD	NC	1061	0.21
	HT	823	0.31
	HM	552	0.46
Volume	NC	828	0.34
	HT	661	0.42
	HM	430	0.52

We computed the required MSS of three longitudinal groups from baseline to 24-month follow-up based on UMIs, UMI-RDs, and volume measures, respectively. The comparison results are shown in Table 4. Paired Cohen's d measure computes the effect sizes of the three longitudinal groups. For the longitudinal NC, HT, and HM groups, the MSSs and effect sizes for UMIs mean differences are 533 and

Table 5
Mean R_f values of different biomarkers comparisons between different longitudinal genotype groups (from the AZ *APOE* cohort)

Biomarker	Group Comparisons	Average R_f (%) ± Std (%)	Inferential Statistical
UMI	NC versus HM	0.30 ± 0.87 versus 0.98 ± 1.04	$F = 11.99$; $p = 0.0008$
	NC versus HT	0.30 ± 0.87 versus 0.64 ± 0.64	$F = 5.3$; $p = 0.023$
	HT versus HM	0.64 ± 0.64 versus 0.98 ± 1.04	$F = 4.05$; $p = 0.048$
UMI-RD	NC versus HM	0.03 ± 0.08 versus 0.09 ± 0.20	$F = 4.14$; $p = 0.045$
	NC versus HT	0.03 ± 0.08 versus 0.03 ± 0.03	$F = 2.18$; $p = 0.14$
	HT versus HM	0.03 ± 0.03 versus 0.09 ± 0.20	$F = 1.84$; $p = 0.18$
volume	NC versus HM	-0.01 ± 0.04 versus -0.05 ± 0.08	$F = 9.89$; $p = 0.0023$
	NC versus HT	-0.01 ± 0.04 versus -0.03 ± 0.06	$F = 4.61$; $p = 0.041$
	HT versus HM	-0.03 ± 0.06 versus -0.05 ± 0.08	$F = 2.21$; $p = 0.14$

0.48, 393 and 0.53, 296 and 0.61. For UMI-RDs, the MSSs and effect sizes of the longitudinal NC, HT, and HM groups are 1061 and 0.21, 823 and 0.31, 552 and 0.46. For hippocampal volume measures, the MSSs and effect sizes of the longitudinal NC, HT, and HM groups are 828 and 0.34, 661 and 0.42, 430 and 0.52. This indicates that UMI, as a univariate morphometry biomarker, has more substantial statistical discrimination power to distinguish the longitudinal groups with different *APOE* ε4 genotypes than both the UMI-RDs and the hippocampal volume measures.

Dose effects of APOE ε4 alleles on the longitudinal hippocampal morphological changes

To further validate the *APOE* ε4 allele dose effects on the longitudinal hippocampal atrophies, the ANOVA method is applied on the UMI, UMI-RD, and volume measurement changes between NC and HT, NC and HM, and HT and HM, respectively. The biomarker changes are described as the change rates (R_f) of the biomarker.

$$R_f = \frac{f_{second} - f_{first}}{f_{first}} \tag{6}$$

where f_{first} and f_{second} represent the values of the biomarkers at the baseline test and a 24-month test. We computed the R_f values of UMIs, UMI-RDs, and volume measurements of three longitudinal groups with different *APOE* ε4 genotypes, respectively. The statistical results (shown in Table 5) show that the mean R_f values of the UMIs and UMI-RDs have an upward trend while the mean R_f values of the volume measures have a downward trend from NC to HT to HM genotype. This means that different *APOE* ε4 allele load affects the shrinkage rate of the hippocampus, i.e., HM genotype will cause the largest atrophy rate, followed by HT, and the smallest is NC.

The statistical results for mean R_f values comparisons between different longitudinal genotype groups are computed by the ANOVA method. For the mean R_f values comparisons of NC versus HM, NC versus HT, and HT versus HM, the p-values for UMIs are 0.0008, 0.023, and 0.048, respectively. For UMI-RDs, the p-values are 0.045, 0.14, and 0.18, respectively. For volume measurements, the p-values are 0.0023, 0.041, and 0.14, respectively. The results indicate that the UMIs may have a stronger discrimination ability to distinguish the mean R_f value differences between the three longitudinal groups than both the UMI-RDs and the hippocampal volume measures. With the help of UMI biomarker, i.e., the sensitivity for detecting hippocampal morphological change, we detected the significant group differences for NC versus HM, NC versus HM, and HT versus HM based on the mean R_f values. This indicates that *APOE* ε4, as a major genetic risk factor for AD, affects the hippocampal morphological changes of elderly cognitively unimpaired individuals. In addition, the mean R_f values of HM are larger than those of both HT and NC, i.e., hippocampal atrophy rate of HM > hippocampal atrophy rate of HT > hippocampal atrophy rate of NC, which indicates a clear dose effect of *APOE* ε4 alleles on longitudinal hippocampal atrophy rates. This finding is consistent with prior studies [13, 14, 19, 25, 59–63]. However, there are no significant group differences about mean R_f values of HM versus HT based on volume measurements. There are no significant group differences about mean R_f values of HM versus HT and HT versus NC based on UMI-RDs. This demonstrates that the UMIs based on subspace decomposition may outperform the volume measures and UMI-RDs in distinguishing cognitively unimpaired *APOE* ε4 carriers from NC.

Table 6
The estimated multiple regression coefficients and *p*-values of the multiple regression model (with data from the AZ *APOE* cohort)

Regression Factor	Regression Coefficient	*p*
(Intercept)	–0.084	0.18
Genetic-HT	0.040	0.045
Genetic-HM	0.054	0.0046
Age	0.0023	0.020
Gender-male	0.012	0.45

Multiple R-squared: 0.23

Table 7
The estimated multiple regression coefficients and *p*-values of the modified multiple regression model (with data from the AZ *APOE* cohort)

Regression Factor	Regression Coefficient	*p*
Genetic-HT	0.0012	0.96
Genetic-HM	0.0082	0.68
Age	0.0017	0.31
Gender-male	0.013	0.37
Genetic-HT:Age-group-H	0.062	5.6e-03
Genetic-HM:Age-group-H	0.17	1.11e-05

Multiple R-squared: 0.28

Multiple regression analysis

The effect of *APOE* ε4 allele load on hippocampal morphology in the healthy population is complicated. For example, the *APOE* ε4 allele interacts with specific age-associated pathogenic factors [9]. Some significant interactions with age have been reported in the literature [25, 64] that the effects of *APOE* ε4 allele load on hippocampal morphology of individuals in different aged groups are different. Therefore, the question is whether the calculated UMIs can still reflect the different morphological atrophies associated with different *APOE* ε4 allele loads, considering the individual age and gender factors. Specifically, it is beneficial to see if R_f values of UMIs vary systematically as the copies of the risk allele change. We generate the multiple regression model to test the relationship between R_f values of UMIs and the influence factors including different *APOE* ε4 genetic variances (HM, HT, and NC), age, and gender, i.e., the R_f values of UMIs are taken as dependent variables and the influence factors are taken as independent variables. In this multiple regression model, the genetic variances (i.e., HM, HT, and NC) are transformed into three independent dummy regressors. The estimated regression coefficients and *p*-values of all the regression factors are shown in Table 6.

As we expected, changes in genetic factors are closely related to R_f values of UMIs. As shown in Table 6, taking the *APOE* ε4 non-carriers as a reference genetic group, the average R_f values of UMIs of the HT genetic group increase by 0.040, and the R_f values of UMIs of the HM group increase by 0.054. And the regression coefficients of these two regressors are statistically significant. Moreover, the regression coefficient of the HM group is larger than the one of HT group based on the multiple regression model, which indicates that hippocampal atrophy rate of HM > hippocampal atrophy rate of HT > hippocampal atrophy rate of NC under the influence of age and gender. The results also show that the factor of age has a significant influence on the R_f values of UMIs, i.e., the regression coefficient of the age factor is 0.0023, and the *p*-value of the age factor is 0.020. This indicates that the factor of age also has a significant impact on UMIs, i.e., UMIs tend to increase with aging. In addition, the regression coefficient of male subjects equals 0.012 when female subjects are used as the reference variables, i.e., the average R_f values of UMIs of male subjects with the same age and genetic group is 0.012 greater than female subjects. The results also indicate that there is no significant correlation between UMIs and gender.

To further verify whether the effects of *APOE* ε4 allele load on hippocampal morphology of individuals in different aged groups are different, we add a binary indicator variable (Age-group) to each individual, which is transformed from the age variable. When the individual's age is over 65, the binary indicator is set to high (Age-group-H). Otherwise, it is set to low (Age-group-L). Moreover, we added an interaction term between genetic and Age-group variables to the regression model to test whether the interaction will significantly impact UMIs. The estimated regression coefficients and *p*-values of all the regression factors are shown in Table 7.

The results show that the multiple R-square values of the new multiple regression model increased from 0.23 to 0.28 compared with the multiple regression model in Table 6, indicating that the new model can better explain the R_f values of UMIs. The regression coefficients of the new multiple regression model show that the interaction between *APOE* ε4 genetic factors and age factor has a significant impact on the R_f values of UMIs. For example, in the HT group, the average R_f values of UMIs of all the individuals increase 0.0012 compared with the NC group, and *APOE* ε4 HT genotype will produce an additional R_f value of UMIs with 0.062 for individuals of high age (greater than 65 years old). Similarly,

Table 8
Mean R_f values of different biomarkers comparisons between different longitudinal genotype groups based on ANOCOVA method (from the AZ *APOE* cohort)

Biomarker	Group Comparisons	Inferential Statistical
UMI	NC versus HM	$F = 12.82$; $p = 0.0006$
	NC versus HT	$F = 4.87$; $p = 0.029$
	HT versus HM	$F = 5.23$; $p = 0.025$
UMI-RD	NC versus HM	$F = 4.43$; $p = 0.038$
	NC versus HT	$F = 2.75$; $p = 0.10$
	HT versus HM	$F = 2.19$; $p = 0.15$
volume	NC versus HM	$F = 11.01$; $p = 0.0013$
	NC versus HT	$F = 4.55$; $p = 0.035$
	HT versus HM	$F = 2.79$; $p = 0.099$

Table 9
Mean R_f values of UMI comparisons between different longitudinal genotype groups with three age intervals (from the AZ *APOE* cohort)

Age Group	Group Comparisons	Inferential Statistical
50∼60	NC versus HM	$F = 1.98$; $p = 0.17$
	NC versus HT	$F = 0.13$; $p = 0.72$
	HT versus HM	$F = 0.87$; $p = 0.35$
60∼70	NC versus HM	$F = 2.78$; $p = 0.11$
	NC versus HT	$F = 1.85$; $p = 0.18$
	HT versus HM	$F = 1.46$; $p = 0.24$
70∼80	NC versus HM	$F = 20.83$; $p = 0.0004$
	NC versus HT	$F = 6.61$; $p = 0.018$
	HT versus HM	$F = 7.57$; $p = 0.013$

Significance of gene × age on the R_f values of UMIs

in the HM group, the average R_f value of UMIs increase 0.0082 compared with the NC group, and the *APOE* ε4 HM genotype will produce an additional R_f value of UMIs with 0.17 for individuals of high age (greater than 65 years old). These results may indicate that *APOE* ε4 will accelerate the change of UMIs in the high age population, especially those among HM group, thereby causing the deterioration of the individual's cognitive status, consistent with observations in prior research [65, 66].

Influence of age on the effect of APOE ε4 allele load

As described previously, the factor of age has a significant influence on the effects of *APOE* ε4 allele load on hippocampal morphology of individuals. It is natural to verify what happens to the mean R_f values of different biomarkers comparisons between different longitudinal genotype groups while considering the variable age as a continuous covariate. We further conducted analysis of covariance (ANOCOVA) analysis of experimental data above and the results were shown in Table 8. Compared with Table 5, most of the results are similar except for the detection of more significant group differences between HT and HM groups based on UMIs. For the mean R_f values comparisons of NC versus HM, NC versus HT, and HT versus HM, the p-values for UMIs are 0.0006, 0.029, and 0.025, respectively. For UMI-RDs, the p-values are 0.038, 0.10 and 0.15, respectively. For volume measurements, the p-values are 0.0013, 0.035 and 0.099, respectively. In short, after excluding the influence of individual age differences, we can still find the existence of a clear dose effects of *APOE* ε4 alleles on longitudinal hippocampal atrophy rates.

To answer whether there is a certain age group that whose R_f value is most informative, we divided the individual ages at baseline test into three age groups, i.e., 50∼60, 60∼70, and 70∼80 age groups, and then compared the mean R_f values of UMI biomarker between different longitudinal genotype groups. The comparison results are shown in Table 9. It illustrated that there are no significant group differences about mean R_f values of UMI biomarker for HM versus NC, HT versus NC, and HM versus HT within 50∼60 and 60∼70 age intervals. The mean R_f values of UMI comparisons of NC versus HM, NC versus HT, and HT versus HM, the p-values are 0.17, 0.72, and 0.35 within 50∼60 age interval, respectively. Within 60∼70 age interval, the p-values are 0.11, 0.18, and 0.24, respectively. Within 70∼80 age interval, we find more significant group differences between the three longitudinal genotype groups, i.e., the p-values are 0.0004, 0.018, and 0.013, respectively. This may indicate that the dose effect of *APOE* ε4 alleles on longitudinal hippocampal atrophy rates become more pronounced in the elder age population.

As described above, the factor of age has a significant influence on the R_f values of UMIs, i.e., UMIs tend to increase with aging. We want to study whether the relationship between the R_f values of UMIs and the *APOE* ε4 allele loads depend on the level of individual age. We examined the interactive effect of *APOE* ε4 allele load by age on the R_f values of UMIs in our Arizona *APOE* cohort with regard to *APOE* ε4 HM, HT, and NC by using general linear regression model including the term of age, the term of gene (*APOE* ε4 HM, HT, and NC) and the interaction term of gene by age. The estimated regression coefficients (the corresponding p-values) of age, gene, and age × gene are 0.0054 (0.0098), 0.21 (0.028), and –0.0035 (0.026). The results showed that the interaction term of *APOE* ε4 allele load by age is statistically significant. It indicated that the relationship between

Table 10
Group difference comparisons of different biomarkers at baseline tests (from the AZ *APOE* cohort)

Biomarker	Group Comparisons	Average Baseline ± Std	Inferential Statistical
UMI	NC versus HM	11.11 ± 3.03 versus 12.45 ± 3.21	F = 3.85; p = 0.053
	NC versus HT	11.11 ± 3.03 versus 11.28 ± 2.98	F = 0.09; p = 0.77
	HT versus HM	11.28 ± 2.98 versus 12.45 ± 3.21	F = 2.76; p = 0.10
UMI-RD	NC versus HM	10.83 ± 3.22 versus 11.42 ± 5.12	F = 0.45; p = 0.50
	NC versus HT	10.83 ± 3.22 versus 11.04 ± 4.27	F = 0.08; p = 0.80
	HT versus HM	11.04 ± 4.27 versus 11.42 ± 5.12	F = 0.13; p = 0.72
Volume × 1000	NC versus HM	9.924 ± 0.89 versus 9.933 ± 0.91	F = 0; p = 0.96
	NC versus HT	9.924 ± 0.89 versus 9.931 ± 1.04	F = 0; p = 0.97
	HT versus HM	9.931 ± 1.04 versus 9.933 ± 0.91	F = 0; p = 0.99

the R_f values of UMIs and gene differs depending on the ages of individuals.

Group difference comparisons at baseline tests

To verify whether there is any difference among NC, HT, and HM on the baseline of UMI, UMI-RD, and volume measurements, we used the UMIs, UMI-RDs, and volume measures at the baseline test from the AZ *APOE* cohort, i.e., 140 cognitively unimpaired individuals including 61 NCs, 49 HTs, and 30 HMs, and applied significant test of group mean differences between NC and HT, NC and HM, and HT and HM based on the ANOVA method. The results shown in Table 10 indicated that there are no significant group mean differences between NC and HT, NC and HM, and HT and HM by using these three biomarkers at baseline test. These cross-sectional findings are consistent with observations in prior research [28–30]. The results completed our study and demonstrated the superior sensitivity gained from our novel framework.

Correlation analysis with volume and cognitive outcomes

Although our work is focused on *APOE* genetic effect analyses, it is natural to verify whether the UMIs are correlated with other imaging and clinical rating scores, such as hippocampal volume, MMSE scores [53], AVLT-LTM scores [54]. Using the Pearson parametric test [67], we explore the correlation analysis between the R_f values of UMIs between the R_f values of hippocampal volume, MMSE, and AVLT-LTM measures, to understand which variables are correlated with UMIs in the AZ *APOE* cohort. The correlation results, i.e., correlation coefficients (CC), 95% confidential intervals of CC, and correlation significance of t-test for CC between the R_f values of UMIs and the R_f values of MMSE, volume, AVLT-LTM measures, are shown in Table 11.

Table 11
The correlation analysis between the R_f values of UMIs and the R_f values of hippocampal volume, MMSE, and AVLT-LTM measures (with data from the AZ *APOE* cohort)

	CC	95% CI of CC	p of CC
UMI versus Hippocampal Volume	–0.80	–0.88∼–0.68	3.43e-12
UMI versus MMSE	–0.13	–0.39∼0.16	0.38
UMI versus AVLT-LTM	–0.11	–0.38∼0.18	0.46

Results indicate that the R_f values of UMIs have strong negative correlations with the R_f values of hippocampal volume measures, i.e., CC is –0.80 (p = 3.43e-12). This is likely due to the UMIs showing an increase with a corresponding hippocampal volume decrease, according to the distributions of UMIs versus volume measurements. In other words, under the influence of the *APOE* ε4 risk allele, the hippocampal volume tends to shrink, and the UMIs obtained by our model has an increasing trend. We have known that the volumetric MRI measurements of the hippocampus are generally accepted as the best-established biomarkers of clinical AD progression. The relationship between UMIs and volume measurements indicates that UMIs may depict the morphological changes induced by AD.

In addition, there is a weak negative correlation between the R_f values of UMIs and the R_f values of MMSE scores, i.e., CC is –0.13 (p = 0.38). With increasing UMIs, the MMSE scores tend to decrease slightly. Similarly, we also did not find a close association between UMIs and AVLT-LTM measures, i.e., CC is –0.11 (p = 0.46). A reasonable reason may be that the morphological changes caused by AD occur before the cognitive decline in the non-destructive cognitive stage, as previously reported in the literature [68, 69].

DISCUSSION

Here we propose a novel univariate morphometry index which is sensitive to AD-induced hippocampal morphometry changes and enjoys improved computational efficiency than our prior work [36]. The newly proposed UMI demonstrated exceptional statistical ability to characterize *APOE* ε4 gene dose effect on longitudinal hippocampal atrophies of elderly cognitively unimpaired individuals with three different experimental designs. UMIs illustrate AD-related morphological changes using a summary index free from the Type I error associated with multiple comparisons. The more prominent the individual has the atrophic morphological characteristics caused by AD in the defined ROI regions, the larger the corresponding UMI value is. Since *APOE* is a significant genetic risk factor for developing AD, its discovery has made it possible to study large numbers of genetically at-risk individuals before the onset of symptomatic memory impairment and has led to the concept of the preclinical stage of AD [5]. A UMI which is sensitive to *APOE* ε4 dose effects will help evaluate AD burden, progression, and response to interventions. Therefore, our work provides a cost-effective and accurate means for prognosis and potentially facilitates enrollment in clinical trials with preclinical AD patients.

In the current work, our main goal is to generate reliable and robust structural MRI ROIs by the analysis of the statistical morphometry difference between the pathology-confirmed AD patients and the pathology-confirmed CU subjects. To address the inhomogeneity of AD pathology, we used the specific AD subjects who had the clinical symptom-based AD diagnosis together with the accumulation of Aβ in brains. As we know, one of the hallmarks of AD is the accumulation of Aβ in human brains and a positive Aβ reading is now accepted as 'dementia due to AD' together with the presence of clinical symptoms. In our previous work [36], the generated ROIs based on the group common structures of Aβ positive AD and Aβ negative CU groups could reflect intrinsic morphological changes induced by AD. And we found that Aβ-induced biomarkers are strong indicator for brain structure atrophy. Therefore, we continued this approach that extracts ROIs from the morphometric difference analysis between Aβ positive patients and Aβ negative subjects. On the other hand, with the same framework, whether features extracted from the morphometric analysis between mild AD patients and CU subjects are more representative of the key initial changes deserves more investigation. However, due to AD's high heterogeneousness, we hypothesize that it is suboptimal to develop a univariate biomarker from the morphometric analysis of mild AD patients.

Even though the proposed UMI based on subspace decomposition could be used to describe the hippocampal morphological changes induced by the *APOE* ε4 risk allele for AD, there are several limitations. First, the relatively small number of subjects are included as the research objects, e.g., the ROIs are extracted from 120 Aβ positive AD patients and 257 Aβ negative CU subjects), which is not enough to characterize the induced general morphological changes induced by AD fully. For example, there is a certain degree of difference for extracting the common group structure under the condition of the limited number of training samples at each time. Therefore, the generated ROIs may be slightly different each time because of different extracted common group structures. It is conceivable that as the sample size gradually increases, the difference in the ROIs caused by the different training samples will be further reduced. Therefore, considering the limitation of the amount of data and the generalization performance of ROIs in applications, we assign the same weight to each point in the ROIs when characterizing the morphological changing regions induced by AD. Secondly, we just chose the RD as the hippocampal morphological feature because RD has been applied in several subcortical studies and served as an ideal description of the hippocampal structural changes induced by AD. However, multivariate tensor-based morphometry (mTBM) [16] is sensitive to deformations such as rotation, dilation, and shear along the surface tangent direction. Therefore, the mTBM can effectively capture hippocampal structural alterations (e.g., atrophy and enlargement) in tensor fields. The ability to describe the morphological features of hippocampi will be enhanced if we combine the mTBM measure and the RD measure. In addition to morphological characteristics, some core AD (i.e., Aβ and tau) biomarkers are needed to construct the biological mechanisms underlying our findings in hippocampal morphology measurements.

Conclusion and future work

A univariate morphometry biomarker generation method is proposed based on subspace decomposition to effectively depict the hippocampal morphological changes induced by three levels of genetic risk for AD. The empirical results

demonstrated the potential that the UMIs may capture the *APOE* ε4 risk allele-induced brain morphometry abnormalities and reveal the dose effects of *APOE* ε4 on the hippocampal morphology in cognitively normal individuals. In our future work, we will devise a tensor field data-based univariate morphometry biomarker which may be applied to analyze diffusion tensor imaging data for the differential diagnosis, early detection and tracking, and the prediction of clinical decline before the onset stage of AD.

ACKNOWLEDGMENTS

This work was partially supported by National Natural Science Foundation of China (62171209, 61772253, 61771231, 61872170, 61877065, 6187 3117, 81571234); Key Research and Development Program of Shandong Province (2019JZZY 010125); Key Project of Shandong Natural Science Foundation (ZR2020KF023); National Institute on Aging (R21AG065942, R01AG069453, and P30AG 072980), the National Institute for Biomedical Imaging and Bioengineering (R01EB025032), National Eye Institute (R01EY032125), National Institute of Dental & Craniofacial Research (R01DE030286), and the Arizona Alzheimer Consortium.

Data collection and sharing for this project was funded by the Alzheimer's Disease Neuroimaging Initiative (ADNI) (National Institutes of Health Grant U01 AG024904) and DOD ADNI (Department of Defense award number W81XWH-12-2-0012). ADNI is funded by the National Institute on Aging, the National Institute of Biomedical Imaging and Bioengineering, and through generous contributions from the following: AbbVie, Alzheimer's Association; Alzheimer's Drug Discovery Foundation; Araclon Biotech; BioClinica, Inc.; Biogen; Bristol-Myers Squibb Company; CereSpir, Inc.; Cogstate; Eisai Inc.; Elan Pharmaceuticals, Inc.; Eli Lilly and Company; EuroImmun; F. Hoffmann-La Roche Ltd and its affiliated company Genentech, Inc.; Fujirebio; GE Healthcare; IXICO Ltd.;Janssen Alzheimer Immunotherapy Research & Development, LLC.; Johnson & Johnson Pharmaceutical Research & Development LLC.; Lumosity; Lundbeck; Merck & Co., Inc.;Meso Scale Diagnostics, LLC.; NeuroRx Research; Neurotrack Technologies; Novartis Pharmaceuticals Corporation; Pfizer Inc.; Piramal Imaging; Servier; Takeda Pharmaceutical Company; and Transition Therapeutics. The Canadian Institutes of Health Research is providing funds to support ADNI clinical sites in Canada. Private sector contributions are facilitated by the Foundation for the National Institutes of Health (http://www.fnih.org). The grantee organization is the Northern California Institute for Research and Education, and the study is coordinated by the Alzheimer's Therapeutic Research Institute at the University of Southern California. ADNI data are disseminated by the Laboratory for Neuro Imaging at the University of Southern California.

Authors' disclosures available online (https://www.j-alz.com/manuscript-disclosures/21-5149r2).

SUPPLEMENTARY MATERIAL

The supplementary material is available in the electronic version of this article: https://dx.doi.org/10.3233/JAD-215149.

REFERENCES

[1] Caselli RJ, Reiman EM (2012) Characterizing the preclinical stages of Alzheimer's disease and the prospect of presymptomatic intervention. *J Alzheimers Dis* **33**, 405-416.

[2] Langbaum JB, Fleisher AS, Chen K, Ayutyanont N, Lopera F, Quiroz YT, Caselli RJ, Tariot PN, Reiman EM, (2013) Ushering in the study and treatment of preclinical Alzheimer disease. *Nat Rev Neurol* **9**, 371-381.

[3] Corder EH, Saunders AM, Strittmatter WJ, Schmechel DE, Gaskell PC, Small GW, Roses AD, Haines JL, Pericakvance MA (1993) Gene dose of apolipoprotein E type 4 allele and the risk of Alzheimer's disease in late onset families. *Science* **261**, 921-923.

[4] Saunders AM, Strittmatter WJ, Schmechel D, George-Hyslop PH, Pericak-Vance MA, Joo SH, Rosi BL, Gusella JF, Crapper-MacLachlan DR, Alberts MJ (1993) Association of apolipoprotein E allele epsilon 4 with late-onset familial and sporadic Alzheimer's disease. *Neurology* **43**, 1467-1472.

[5] Sperling RA, Aisen PS, Beckett LA, Bennett DA, Craft S, Fagan AM, Iwatsubo T, Jack CR, Kaye J, Montine TJ, Park DC, Reiman EM, Rowe CC, Siemers E, Stern Y, Yaffe K, Carrillo MC, Thies B, Morrison-Bogorad M, Wagster MV, Phelps CH (2011) Toward defining the preclinical stages of Alzheimer's disease: Recommendations from the National Institute on Aging-Alzheimer's Association workgroups on diagnostic guidelines for Alzheimer's disease. *Alzheimers Dement* **7**, 280-292.

[6] Chen K, Reiman EM, Alexander GE, Caselli RJ, Gerkin R, Bandy D, Domb A, Osborne D, Fox N, Crum WR, Saunders AM, Hardy J (2007) Correlations between apolipoprotein E epsilon4 gene dose and whole brain atrophy rates. *Am J Psychiatry* **164**, 916-921.

[7] Reiman EM, Caselli RJ, Yun LS, Chen K, Osborne D (1996) Preclinical evidence of Alzheimer's disease in persons homozygous for the epsilon 4 allele for apolipoprotein E. *N Engl J Med* **334**, 752-758.

[8] Reiman EM, Chen K, Alexander GE, Caselli RJ, Bandy D, Osborne D, Saunders AM, Hardy J (2005) Correlations

between apolipoprotein E epsilon4 gene dose and brain-imaging measurements of regional hypometabolism. *Proc Natl Acad Sci U S A* **102**, 8299-8302.

[9] Chen K, Roontiva A, Thiyyagura P, Lee W, Liu XF, Ayutyanont N, Protas H, Luo JL, Bauer R, Reschke C, Bandy D, Koeppe RA, Fleisher AS, Caselli RJ, Landau S, Jagust WJ, Weiner MW, Reiman EM (2015) Improved power for characterizing longitudinal amyloid-beta PET changes and evaluating amyloid-modifying treatments with a cerebral white matter reference region. *J Nucl Med* **56**, 560-566.

[10] Kuang L, Jia J, Zhao D, Xiong F, Han X, Wang Y, Alzheimer's Disease Neuroimaging Initiative (2020) Default mode network analysis of APOE genotype in cognitively unimpaired subjects based on persistent homology. *Front Aging Neurosci* **12**, 188.

[11] Fox NC, Scahill RI, Crum WR, Rossor MN (1999) Correlation between rates of brain atrophy and cognitive decline in AD. *Neurology* **52**, 1687-1687.

[12] Josephs KA, Whitwell JL, Ahmed Z, Shiung MM, Weigand SD, Knopman DS, Boeve BF, Parisi JE, Petersen RC, Dickson DW, Jack CR (2008) Beta-amyloid burden is not associated with rates of brain atrophy. *Ann Neurol* **63**, 204-212.

[13] Reiman EM, Uecker A, Caselli RJ, Lewis S, Bandy D, Leon MD, De SS, Convit A, Osborne D, Weaver AL, Thibodeau SN (1998) Hippocampal volumes in cognitively normal persons at genetic risk for Alzheimer's disease. *Ann Neurol* **44**, 288-291.

[14] Thompson PM, Hayashi KM, Zubicaray G, Janke AL, Rose SE, Semple J, Hong MS, Herman D, Gravano D, Doddrell DM, Toga AW (2004) Mapping hippocampal and ventricular change in Alzheimer's disease. *Neuroimage* **22**, 1754-1766.

[15] Jack CR, Slomkowski M, Gracon S, Hoover TM, Felmlee JP, Stewart K, Xu Y, Shiung M, O'Brien PC, Cha R, Knopman DS, Petersen RC (2003) MRI as a biomarker of disease progression in a therapeutic trial of milameline for AD. *Neurology* **60**, 253-260

[16] Wang Y, Song Y, Rajagopalan P, An T, Liu K, Chou YY, Gutman BA, Toga AW, Thompson PM (2011) Surface-based TBM boosts power to detect disease effects on the brain: An *N*=804 ADNI study. *Neuroimage* **56**, 1993-2010.

[17] Soininen H, Partanen K, Pitkanen A, Hallikainen M, Hanninen T, Helisalmi S, Mannermaa A, Ryynanen M, Koiuisto K, Riekkinen P (1995) Decreased hippocampal volume asymmetry on MRIs in nondemented elderly subjects carrying the apolipoprotein E epsilon 4 allele. *Neurology* **45**, 391-392.

[18] Wang L, Swank JS, Glick IE, Gado MH, Miller M, Morris JC, Csernansky JG (2003) Changes in hippocampal volume and shape across time distinguish dementia of the Alzheimer type from healthy aging. *Neuroimage* **20**, 667-682.

[19] Shen L, Firpi H, Saykin AJ, West JD (2009) Parametric surface modeling and registration for comparison of manual and automated segmentation of the hippocampus. *Hippocampus* **19**, 588-595.

[20] Kerchner GA, Berdnik D, Shen JC, Bernstein JD, Fenesy MC, Deutsch GK, Wyss-Coray T, Rutt BK (2014) APOE epsilon4 worsens hippocampal CA1 apical neuropil atrophy and episodic memory. *Neurology* **82**, 691-697.

[21] Filippini N, Rao A, Wetten S, Gibson RA, Borrie M, Guzman D, Kertesz A, Loy-English I, Williams J, Nichols TE, Whitcher B, Matthews PM (2009) Anatomically-distinct genetic associations of APOE epsilon4 allele load with regional cortical atrophy in Alzheimer's disease. *Neuroimage* **44**, 724-728.

[22] Chen KL, Sun YM, Zhou Y, Zhao QH, Ding D, Guo QH (2016) Associations between APOE polymorphisms and seven diseases with cognitive impairment including Alzheimer's disease, frontotemporal dementia, and dementia with Lewy bodies in southeast China. *Psychiatr Genet* **26**, 124-131.

[23] Saeed U, Mirza SS, MacIntosh BJ, Herrmann N, Keith J, Ramirez J, Nestor SM, Yu Q, Knight J, Swardfager W, Potkin SG, Rogaeva E, George-Hyslop PS, Black SE, Masellis M (2018) APOE-ε4 associates with hippocampal volume, learning, and memory across the spectrum of Alzheimer s disease and dementia with Lewy bodies. *Alzheimers Dement* **14**, 1137-1147.

[24] Hostage CA, Choudhury KR, Doraiswamy PM, Petrella JR (2013) Dissecting the gene dose-effects of the APOE ε4 and ε2 alleles on hippocampal volumes in aging and Alzheimer's disease. *PLoS One* **8**, e54483.

[25] Cacciaglia R, Molinuevo JL, Falcón C, Brugulat-Serrat A, Sánchez-Benavides G, Gramunt N, Esteller M, Morán S, Minguillón C, Fauria K (2018) Effects of APOE-ε4 allele load on brain morphology in a cohort of middle-aged healthy individuals with enriched genetic risk for Alzheimer's disease. *Alzheimers Dement* **14**, 902-912.

[26] Martí-Juan G, Sanroma-Guell G, Cacciaglia R, Falcon C, Piella G (2020) Nonlinear interaction between APOE ε4 allele load and age in the hippocampal surface of cognitively intact individuals. *Hum Brain Mapp* **42**, 47-64.

[27] Dong Q, Zhang W, Wu J, Li B, Schron EH, Mahon TM, Shi Jie, Gutman BA, Chen K, Baxter LC, Thompson PM, Reiman EM, Caselli RJ, Wang Y (2019) Applying surface-based hippocampal morphometry to study APOE-E4 allele dose effects in cognitively unimpaired subjects. *Neuroimage* **22**, 101744.

[28] Protas HD, Chen K, Langbaum JBS, Fleisher AS, Alexander GE, Lee W, Bandy D, Mony J, Mosconi L, Buckley S, Truran-Sacrey D, Schuff N, Weiner MW, Caselli RJ, Reiman EM (2013) Posterior cingulate glucose metabolism, hippocampal glucose metabolism, and hippocampal volume in cognitively normal, late-middle-aged persons at 3 levels of genetic risk for Alzheimer disease. *JAMA Neurol* **70**, 320-325.

[29] Mondadori CRA, Quervain DJF, Buchmann A, Mustovic H, Wollmer MA, Schmidt CF, Boesiger P, Hock C, Nitsch RM, Papassotiropoulos A, Henke K (2007) Better memory and neural efficiency in young apolipoprotein E epsilon4 carriers. *Cereb Cortex* **17**, 1934-1947.

[30] Burggren AC, Zeineh M, Ekstrom AD, Braskie MN, Thompson PM, Small GW, Bookheimer SY (2008) Reduced cortical thickness in hippocampal subregions among cognitively normal apolipoprotein E e4 carriers. *Neuroimage* **41**, 1177-1183.

[31] Gonneaud J, Arenaza-Urquijo EM, Fouquet M, Perrotin A, Fradin S, Sayette VDL, Eustache F, Chételat G (2016) Relative effect of APOE ε4 on neuroimaging biomarker changes across the lifespan. *Neurology* **87**, 1696-1703.

[32] Matura S, Prvulovic D, Jurcoane A, Hartmann D, Miller J, Scheibe M, Odwyer L, Oertelknochel V, Knochel C, Reinke B, Karakaya T, Fuser F, Pantel J (2014) Differential effects of the ApoE4 genotype on brain structure and function. *Neuroimage* **89**, 81-91.

[33] Filippini N, MacIntosh BJ, Hough MG, Goodwin GM, Frisoni GB, Smith SM, Matthews PM, Beckmann CF,

Mackay CE (2009) Distinct patterns of brain activity in young carriers of the APOE-epsilon4 allele. *Proc Natl Acad Sci U S A* **106**, 7209-7214.

[34] Sabuncu MR, Ge T, Holmes AJ, Smoller JW, Buckner RL, Fischl B (2016) Morphometricity as a measure of the neuroanatomical signature of a trait. *Proc Natl Acad Sci U S A* **113**, 5749-5756.

[35] Jack CR, Bennett DA, Blennow K, Carrillo MC, Feldman HH, Frisoni GB, Hampel H, Jagust WJ, Johnson KA, Knopman DS, Petersen RC, Scheltens P, Sperling RA, Dubois B (2016) A/T/N: An unbiased descriptive classification scheme for Alzheimer disease biomarkers. *Neurology* **87**, 539-547.

[36] Wang G, Dong QX, Wu JF, Su Y, Chen K, Su QT, Zhang XF, Hao JG, Yao T, Liu L, Zhang CM, Caselli RJ, Reiman EM, Wang YL (2020) Developing univariate neurodegeneration biomarkers with low-rank and sparse subspace decomposition. *Med Image Anal* **67**, 1-16.

[37] Bouwmans T, Zahzah EH, (2014) Robust PCA via principal component pursuit: A review for a comparative evaluation in video surveillance. *Comput Vis Image Underst* **122**, 22-34.

[38] Mueller SG, Weiner MW, Thal LJ, Petersen RC, Jack CR, Jagust WJ, Trojanowski JQ, Toga AW, Beckett LA (2005) The Alzheimer's Disease Neuroimaging Initiative. *Neuroimaging Clin N Am* **15**, 869-877, xi-xii.

[39] Caselli RJ, Reiman EM, Osborne D, Hentz JG, Baxter LC, Hernandez JL, Alexander GG (2004) Longitudinal changes in cognition and behavior in asymptomatic carriers of the APOE e4 allele. *Neurology* **62**, 1990-1995.

[40] Hyman BT (2011) Amyloid-dependent and amyloid-independent stages of Alzheimer disease. *Arch Neurol* **68**, 1062-1064.

[41] Hixson JE, Vernier1 DT (1990) Restriction isotyping of human apolipoprotein E by gene amplification and cleavage with HhaI. *J Lipid Res* **31**, 545-548.

[42] Petersen RC, Doody RS, Kurz A, Mohs RC, Morris JC, Rabins PV, Ritchie K, Rossor MN, Thal LJ, Winblad B (2001) Current concepts in mild cognitive impairment. *JAMA Neurol* **58**, 1985-1992.

[43] Pizer SM, Fritsch DS, Yushkevich PA, Johnson VE, Chaney EL (1999) Segmentation, registration, and measurement of shape variation via image object shape. *IEEE Trans Med Imaging* **18**, 851-865.

[44] Styner M, Oguz I, Xu S, Brechbuhler C, Pantazis D, Levitt JJ, Shenton ME, Gerig G (2006) Framework for the statistical shape analysis of brain structures using SPHARM-PDM. *Insight J*, pp. 242-250.

[45] Patenaude B, Smith SM, Kennedy DN, Jenkinson M (2011) A Bayesian model of shape and appearance for subcortical brain segmentation. *Neuroimage* **56**, 907-922.

[46] Lorensen WE, Cline HE (1987) Marching cubes: A high resolution 3D surface construction algorithm. *ACM SIGGRAPH Comp Graph* **21**, 163-169.

[47] Shi J, Thompson PM, Gutman BA, Wang Y (2013) Surface fluid registration of conformal representation: Application to detect disease burden and genetic influence on hippocampus. *Neuroimage* **78**, 111-134.

[48] Bronielsen M, Gramkow C (1996) Fast fluid registration of medical images. *Microsc Microanal* **28**, 680-681.

[49] Aybat NS, Goldfarb D, Iyengar G (2011) Fast first-order method for stable principal component pursuit. arXiv:1105.2126

[50] Zhou Z, Li XD, Wright J, Candes EJ, Ma Y (2010) Stable principal component pursuit. IEEE International Symposium on Information Theory, pp. 1518-1522.

[51] Cai JF, Candes EJ, Shen Z (2010) A singular value thresholding algorithm for matrix completion. *SIAM J Optim* **20**, 1956-1982.

[52] Gill PMW (2007) Efficient calculation of *p*-values in linear-statistic permutation significance tests. *J Stat Comput Simul* **77**, 55-61.

[53] Folstein MF, Folstein SE, McHugh PR (1975) "Mini-mental state": A practical method for grading the cognitive state of patients for the clinician. *J Psychiatr Res* **12**, 189-198.

[54] Rey A, Reymermet A, Anacona CAR (1964) *L'examen clinique en psychologie*. Presses Universitaires de France, Paris.

[55] Bernard R (2015) *Fundamentals of Biostatistics* (8th edition), Brooks Cole.

[56] Liu G, Yan S (2012) Active subspace: Toward scalable low-rank learning. *Neural comput* **24**, 427-444.

[57] Jack CR, Petersen RC, Xu YC, O'Brien PC, Smith GE, Ivnik RJ, Boeve BF, Waring SC, Tangalos EG, Kokmen E (1999) Prediction of AD with MRI-based hippocampal volume in mild cognitive impairment. *Neurology* **52**, 1397-1397.

[58] Shi J, Stonnington CM, Thompson PM, Chen K, Gutman B, Reschke C, Baxter LC, Reiman EM, Caselli RJ, Wang Y (2015) Studying ventricular abnormalities in mild cognitive impairment with hyperbolic Ricci flow and tensor-based morphometry. *Neuroimage* **104**, 1-20.

[59] Lematre H, Crivello F, Dufouil C, Grassiot B, Mazoyer B (2005) No epsilon4 gene dose effect on hippocampal atrophy in a large MRI database of healthy elderly subjects. *Neuroimage* **24**, 1205-1213.

[60] Crivello F, Lemaitre H, Dufouil C (2010) Effects of ApoE-epsilon4 allele load and age on the rates of grey matter and hippocampal volumes loss in a longitudinal cohort of 1186 healthy elderly persons. *Neuroimage* **47**, 1064-1069.

[61] Styner M, Lieberman JA, Pantazis D, Gerig G (2004) Boundary and medial shape analysis of the hippocampus in schizophrenia. *Med Image Anal* **8**, 197-203.

[62] Morra JH, Tu Z, Apostolova LG, Green AE, Avedissian C, Madsen SK, Parikshak N, Toga AW, Jr CRJ, Schuff N (2009) Automated mapping of hippocampal atrophy in 1-year repeat MRI data from 490 subjects with Alzheimer's disease, mild cognitive impairment, and elderly controls. *Neuroimage* **45**(1 Suppl), S3-15.

[63] Younes L, Albert M, Miller M (2014) Inferring change-point times of medial temporal lobe morphometric change in preclinical Alzheimer's disease. *Neuroimage Clin* **5**, 178-187.

[64] Caselli RJ, Dueck AC, Osborne D, Sabbagh MN, Connor DJ, Ahern GL, Baxter LC, Rapcsak SZ, Shi J, Woodruff BK, Locke DEC, Snyder CH, Alexander GE, Rademakers R, Reiman EM (2009) Longitudinal modeling of age-related memory decline and the APOE epsilon4 effect. *N Engl J Med* **361**, 255-263.

[65] O'Donoghue MC, Murphy SE, Zamboni G, Nobre AC, Mackay CE (2018) APOE genotype and cognition in healthy individuals at risk of Alzheimer's disease: A review. *Cortex* **104**, 103-123.

[66] Laukka EJ, Lovden M, Herlitz A, Karlsson S, Ferencz B, Pantzar A, Kelle L, Graff C, Fratiglioni L, Backman L (2013) Genetic effects on old-age cognitive functioning: A population-based study. *Psychol Aging* **28**, 262-274.

[67] Lemasson B, Christen T, Serduc R, Maisin C, Bouchet A, Duc GL, Remy C, Barbier EL (2012) Evaluation of the relationship between MR estimates of blood oxygen saturation and hypoxia: Effect of an antiangiogenic treatment on a gliosarcoma model. *Radiology* **265**, 743-752.

[68] Jack CR, Bennett DA, Blennow K, Carrillo MC, Dunn B, Haeberlein SB, Holtzman DM, Jagust W, Jessen F, Karlawish J, Liu E, Molinuevo JL, Montine T, Phelps C, Rankin KP, Rowe CC, Scheltens P, Siemers E, Snyder HM, Sperling R, Elliott C, Masliah E, Ryan L, Silverberg N (2018) NIA-AA Research Framework: Toward a biological definition of Alzheimer's disease. *Alzheimers Dement* **14**, 535-562.

[69] Weston PS, Nicholas JM, Lehmann M, Ryan NS, Liang Y, Macpherson K, Modat M, Rossor MN, Schott JM, Ourselin S, Fox NC (2016) Presymptomatic cortical thinning in familial Alzheimer disease: A longitudinal MRI study. *Neurology* **87**, 2050-2057.